Supporting Information

Temperature-tunable optical properties and carrier relaxation of $CuInP_2S_6$ crystal under ferroelectric-paraelectric phase transition

Xiao-Qing Yan,[1,3] Xin Zhao,[2,] Haijie Xu,[1] Lei Zhang,[1] Dongqi Liu,[1] Yuchen Zhang,[1] Changfu Huo,[1] Fang Liu,[1] Junfang Xie,[1] Xiao Dong,[1] Zhi-Bo Liu,[1,*] and Jian-Guo Tian[1,*]*

[1]Key Laboratory of Weak-Light Nonlinear Photonics, Ministry of Education, School of Physics, Nankai University, Tianjin 300071, China

[2]School of Physical Science and Technology, Tiangong University, Tianjin 300387, China

[3]Collaborative Innovation Center of Extreme Optics, Shanxi University, Taiyuan, Shanxi 030006, China

*E-mail: zx2013@tiangong.edu.cn; liuzb@nankai.edu.cn; jjtian@nankai.edu.cn

Contents

S1. XPS of the measured sample

In order to determine the chemical states of the elements, X-ray photoemission spectroscopy (XPS) measurements were performed on the $CuInP_2S_6$ (CIPS) surface. The obtained XPS of different elements (Figure S1) are very close to former reports. [1, 2] The XPS peaks were fitted and the composition of the crystal was determined by referring to the database. The elements are determined to be Cu, In, P and S, respectively. As shown in Figure S1a, the peaks of 932.4 eV and 952.1 eV correspond to the peaks of $2p_{3/2}$ and $2p_{1/2}$ of Cu, respectively. Figure S1b shows that the main peaks at 444.8 eV and 452.4 eV assigned to In $3d_{5/2}$ and In $3d_{3/2}$, respectively. For the P element data (Figure S1c), the two peaks at 131.6 eV ($2p_{3/2}$) and 132.4 eV ($2p_{1/2}$) correspond to the P-P bond and P-S bond vibrations, respectively. The two bond vibrations are assigned to the +3 valence and +5 valence element peak positions. The peak centered at 133.6 eV is from the oxidized P specie on the surface, likely formed upon long-term exposure of the crystal to the air. [3] Besides, the 2p peaks of S element (Figure S1d) are at 161.9 eV ($2p_{3/2}$) and

163.0 eV ($2p_{1/2}$). From these XPS data analysis, we can determine the chemical states as: Cu is +1, In is +3, and P_2S_6 is −4. Furthermore, the Cu:In:S:P stoichiometric ratios from the XPS analysis are determined to be ~0.3:1.0:2.1:4.0, indicating the existence of copper vacancy and interstitial P atom in the measured CIPS sample.

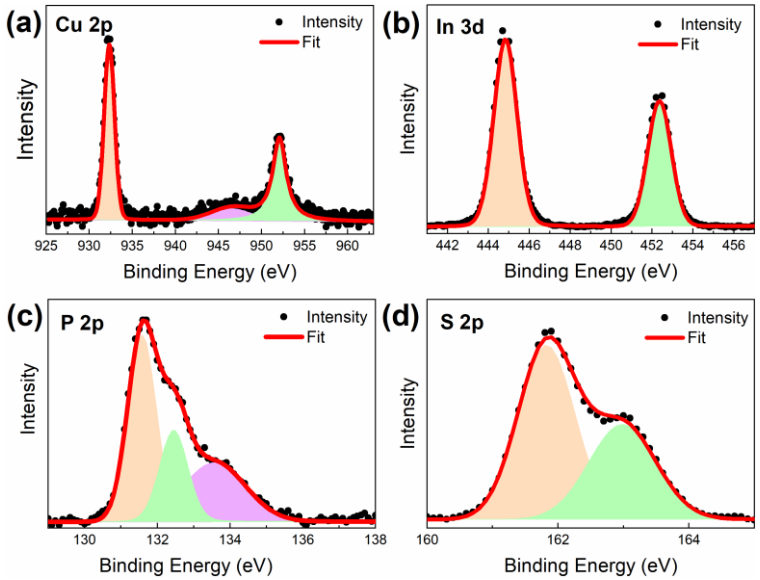

Figure S1. XPS signal of Cu, In, P and S elements, respectively. The circle represents the experimental data, and the solid line represents the fitting.

S2. SEM-EDS results of the measured CIPS crystal

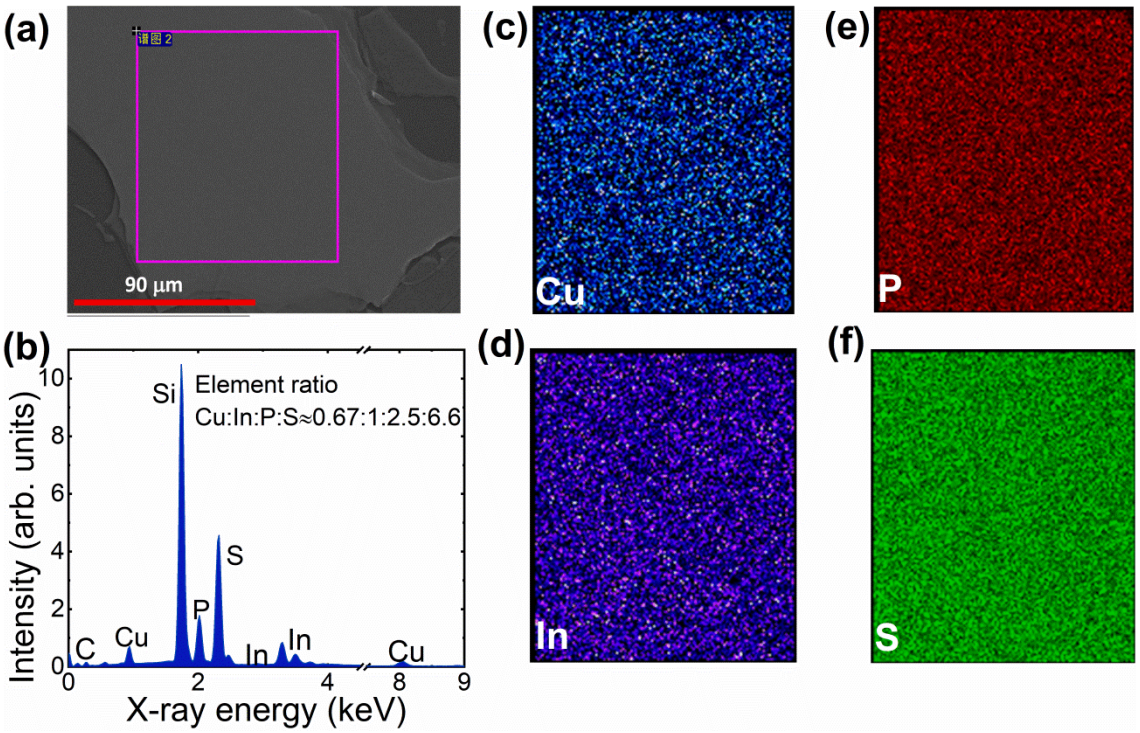

Figure S2. (a) SEM micrograph of the mechanically exfoliated CIPS flake on a silicon wafer. (b) EDS spectrum of the marked area in (a). (c-f) EDS mappings of Cu, In, P, and S elements for the area marked in (a), showing a reasonably homogeneous distribution for all the elements.

Scanning electron microscopy (SEM) and energy dispersive spectroscopy (EDS) were performed for the chemical composition analysis. Morphological images were obtained by using a scanning electron microscope (SEM, Zeiss) equipped with an EDS module for chemical analysis. Figure S2a shows the SEM of a CIPS flake. EDS spectrum indicates the composition of Cu, In, P and S elements in the measured sample (Figure S2b), and the atomic ratio of Cu:In:P:S is measured to be about 0.67:1:2.5:6.6. In addition, EDS imaging reveal the homogeneous distribution for all the elements in the 2D-plane (Figures S2c-S2f), indicating no apparent element accumulation in the measured CIPS crystal. The measured atomic ratio of Cu:In:P:S is different from that from XPS. The more Cu, P and S proportion in the atomic ratio from EDS spectrum may indicate the ununiform distribution of component in different CIPS layers (the sensitive depth of EDS is around μm, while XPS is only sensitive to the near surface region, i.e., a few nanometer). Both XPS and EDS results reveal the deficiency of Cu atom and sufficiency of P atom in the crystal.

S3. In-plane isotropic optical transmittance of CIPS

To explore the in-plane optical anisotropy of CIPS sample, we conducted polarization dependent transmittance measurements by using incident light with wavelength of 532 nm, 633 nm or 800 nm. The light was normally incident into the 2D plane of the sample. As shown in Figure S3, when the polarization of incident light varies from 0° (horizontal) to 90° (vertical), and then to 180° (horizontal), no obvious fluctuation is observed in the transmittance. Therefore, there is no in-plane anisotropy in the optical response of CIPS crystal. This conclusion is supported by the following polarization dependent measurements of PL emission spectra (S6 in this Supporting Information) as well as time-resolved ΔT signal (Figure S11).

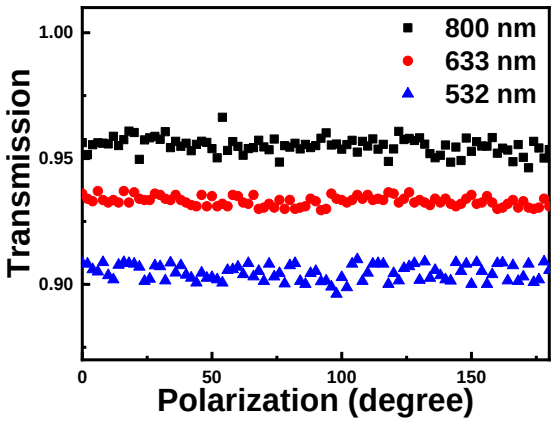

Figure S3. Variation of transmittance with the linear polarization orientation (relative to the horizontal direction) of incident light.

S4. Temperature dependent normalized PL emission spectra

On heating, the PL emission peak shifts slightly towards long wavelength and the emission spectrum broadens a little in the long wavelength region (Figure S4). It indicates that the relative contribution of lower-energy defect-state emission (i.e., the sub-emission with peak at 629 nm) to the PL spectrum enhances slightly at high temperature although the whole PL emission intensity decreases. At high temperature, enhanced carrier-phonon scattering leads to the decrease of radiative recombination contribution to the relaxation of nonequilibrium carriers at the bottoms of defect-bands, and more pronounced for nonequilibrium carriers at energetically higher defect-bands.

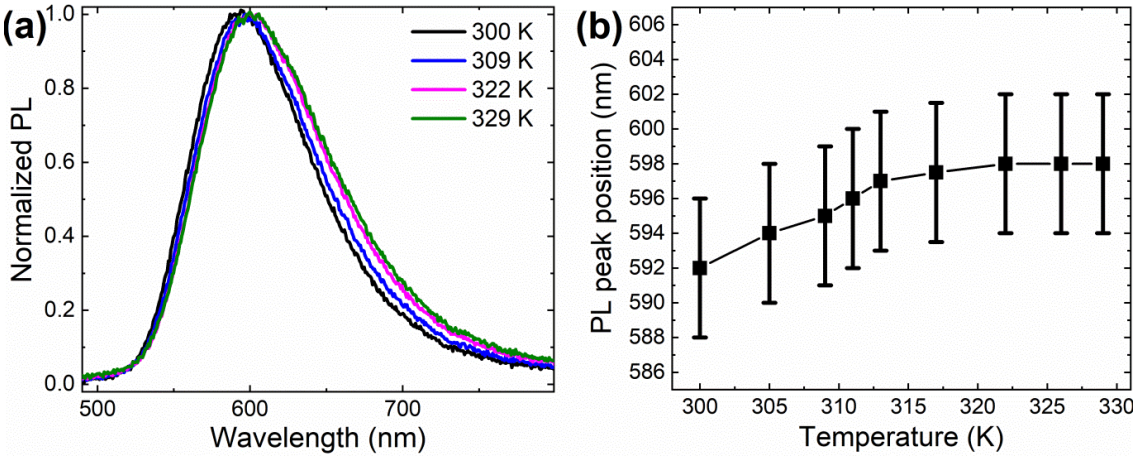

Figure S4. (a) Temperature dependent normalized PL emission spectra under 405nm laser excitation. (b) PL peak position as a function of temperature.

S5. Dependence of PL emission spectrum on the excitation intensity under 532nm laser excitation

As shown in Figure S5, similar to the case of 405nm laser excitation (Figure 2, main text), the PL emission intensity increases as the excitation intensity increases, and saturation behavior of PL emission is observed at high excitation density. In addition, the normalized PL emission spectrum is unchanged with excitation density except some broadening in the long wavelength region, which originates from the noises of excitation light.

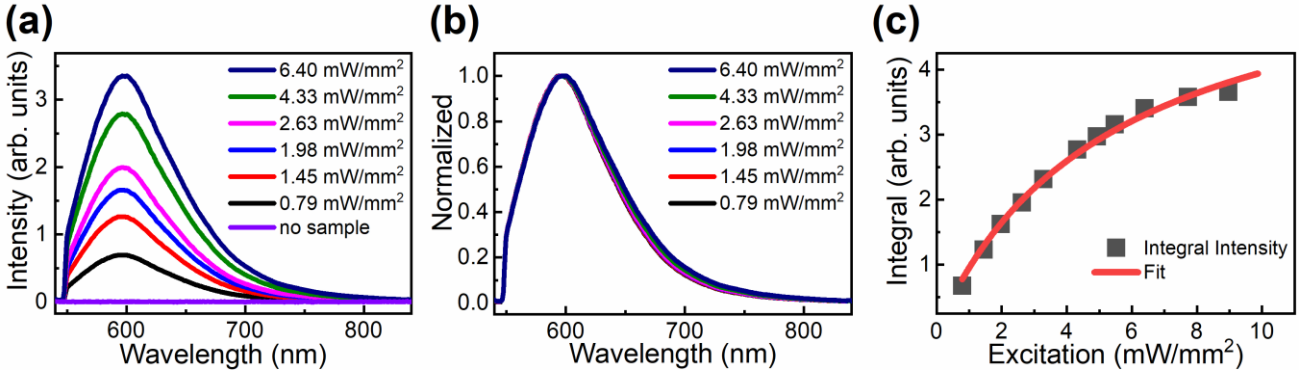

Figure S5. (a) PL emission spectrum of CIPS as a function of the intensity of 532nm excitation light at 295 K. (b) Normalized PL emission spectra for different excitation intensities. The slight broadening observed at

high excitation intensity is from the unfiltered-out noises of excitation light. (c) Integral PL intensity as a function of excitation intensity.

S6. Polarization-independent PL emission spectra under 405nm and 532nm laser excitation

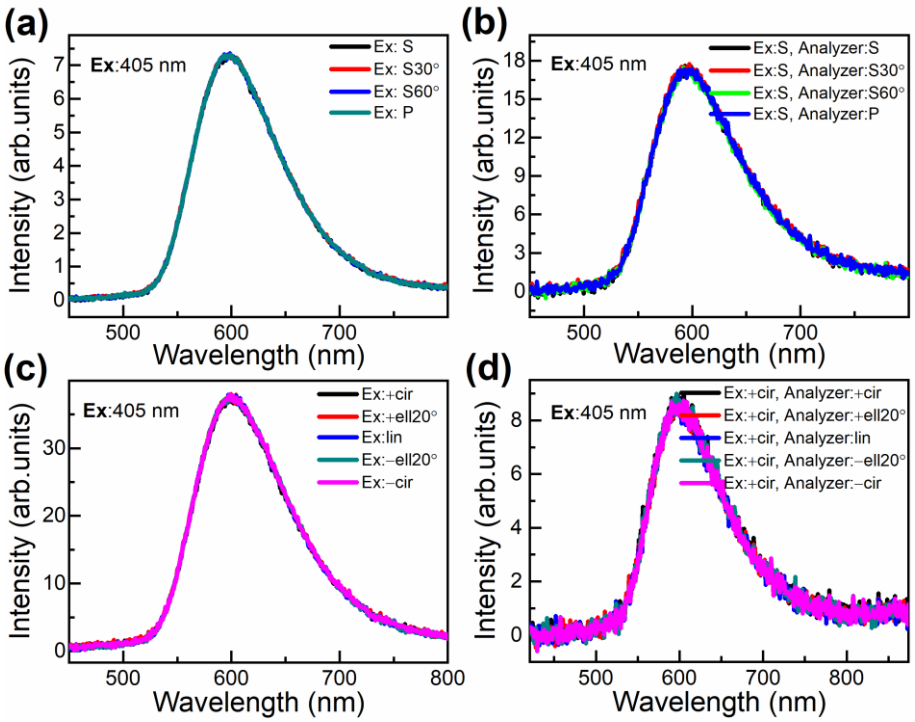

Figure S6. Polarization characteristics of PL emission spectrum under 405nm laser excitation at 295 K. (a) Variation of PL emission spectrum with the linear polarization orientation of excitation light, no analyzer was placed before the detector. S(P) stands for the vertical (horizontal) direction, S30° stands for the linear polarization orientated an angle of 30° with respective to the vertical direction. (b) PL emission spectra after passing through an analyzer with different transmitted polarizations, the excited light was linearly polarized. (c) Dependence of PL emission spectrum on the polarization state of excitation light, the polarization state was changed by an achromatic λ/4 plate and there were no analyzer and λ/4 plate placed before the detector. +/−cir: right/left-handed circular polarization; +/−ell20°: right/left-handed elliptical polarization with a value of tan 20° for the ratio of two polarization ellipse axis. (d) PL emission spectra after passing through an achromatic λ/4 plate and an analyzer, the excited light was right-handed circularly polarized. The polarization of the analyzer was set S, and the achromatic λ/4 plate was altered.

Following, we explore the polarization properties of PL emission spectrum under interband excitation. In the measurement, the sample was excited by using a 405 nm laser. The background noises of excitation light were greatly suppressed by filters, ensuring no clear influence of excitation light noises on the measured PL emission spectrum. To study the dependence of PL emission spectrum on the linear polarization orientation of excitation light, an achromatic λ/2 plate-Glan Taylor prism-achromatic λ/2 plate combination was used to adjust the power and polarization orientation of the linearly polarized excitation light. The second λ/2 plate was replaced by an achromatic λ/4 plate in the measurements of the dependence of PL emission spectrum on the polarization state of excitation light. The emitted light after passing through a set of filters was collected into an Ocean Optics spectrometer.

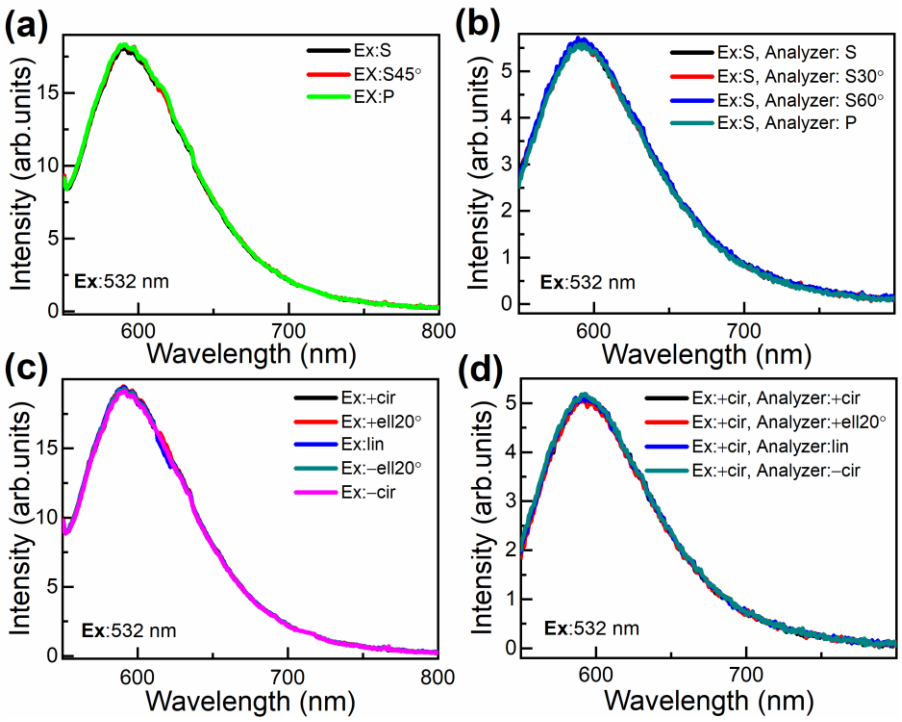

Figure S7. Polarization characteristics of PL emission spectrum under 532nm laser excitation at 295 K. (a) The variation of PL emission spectrum with the linear polarization orientation of excitation light, no analyzer was placed before the detector. (b) PL emission spectra after passing through an analyzer with different transmitted polarizations, the excited light was linearly polarized. (c) Dependence of PL emission spectrum on the polarization state of excitation light, the polarization state was changed by an achromatic λ/4 plate and there were no analyzer and λ/4 plate placed before the detector. (d) PL emission spectra after passing through an achromatic λ/4 plate and an analyzer, the excited light was right-handed circularly polarized. The definitions of the polarizations in these figures are identical to those in Figure S6.

First, we measured the PL emission spectrum by changing the polarization of excitation light. As shown in Figure S6a and S6c, PL emission spectrum does not change with the linear polarization orientation or the polarization state of excitation light, revealing the isotropic optical absorption and no circular dichroism in the 2D plane of CIPS.

To examine the polarization characteristics of emitted light, an analyzer (or an achromatic λ/4 plate and analyzer) was placed before the detector. Under linearly polarized light excitation, the PL emission spectrum does not change with the transmitted-polarization of the analyzer (Figure S6b). If the excited light was right-handed circularly polarized and the transmitted polarization of the analyzer was set S, we adjusted the polarization state of emitted light by rotating the achromatic λ/4 plate placed before the analyzer, the transmitted PL spectrum did not vary at all (Figure S6d). These results indicate that the PL emission excited by linearly or circularly polarized light is without polarization characteristics.

In addition, similar results have been observed in the PL emission spectrum excited by defect-bands absorption (i.e., 532nm laser excitation here, Figure S7).

S7. Pump polarization dependence of ΔT curve from degenerate pump-probe measurements at 800 nm

The ΔT signal during pump excitation is polarization dependent (Figure S8), however, no pump polarization dependence is observed for ΔT signal after pump excitation. It indicates that the ΔT signals of during and after pump excitation originate from different mechanisms. The peak ΔT signal around 0 delay is maximum (minimum) when the pump polarization is parallel (perpendicular) to the probe polarization. As shown in Figures S8 and S9, the ratio of parallel to perpendicular cases is nearly independent on the temperature within experimental error. It is hard to determine precisely the evolution of this ratio with temperature by our measurement system.

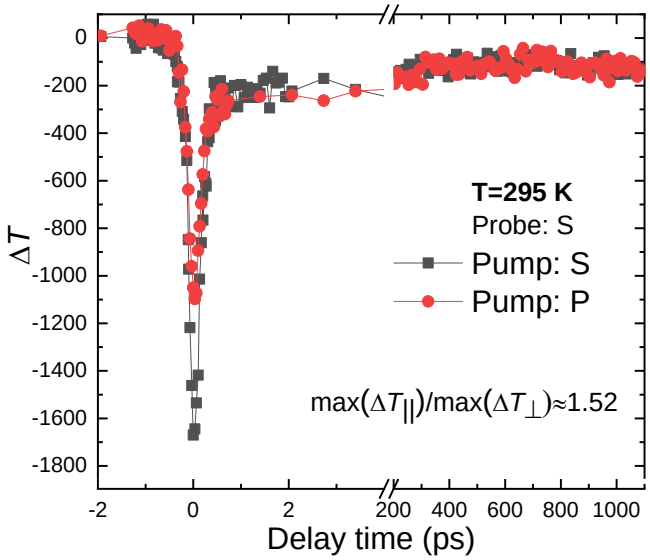

Figure S8. Pump polarization-dependent time-resolved ΔT curve from 800nm-pump 800nm-probe measurements at 295 K, the probe beam is *s*-polarized.

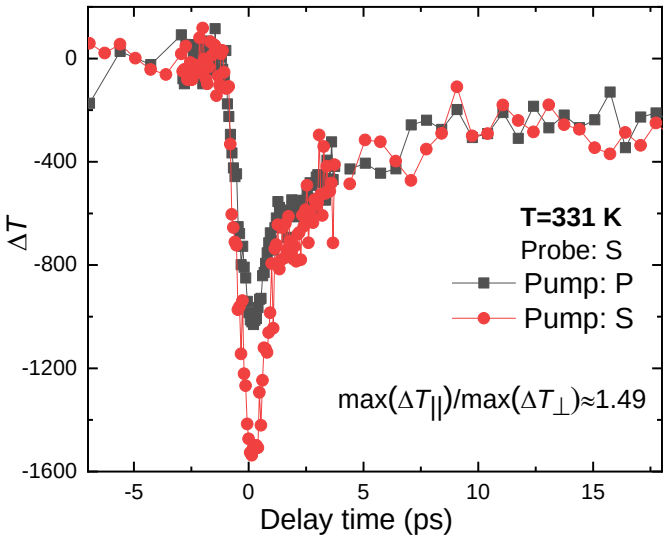

Figure S9. Pump polarization-dependent time-resolved ΔT curve from 800nm-pump 800nm-probe measurements at 331 K, the probe beam is *s*-polarized.

S8. Dependence of ΔT curve on the pump fluence and pump polarization from 400nm-pump 800nm-probe measurements

First, we explore the carrier dynamics via changing the photoexcited carrier density. The carrier density was modulated by pump fluence. Figure S10 shows that the ΔT curve varies with the pump fluence as follows: the peak ΔT signal around 0 delay is proportional to the pump fluence, but the normalized ΔT curve is independent on the pump fluence. Thus, the carrier relaxation process of CIPS is nearly independent on the carrier density.

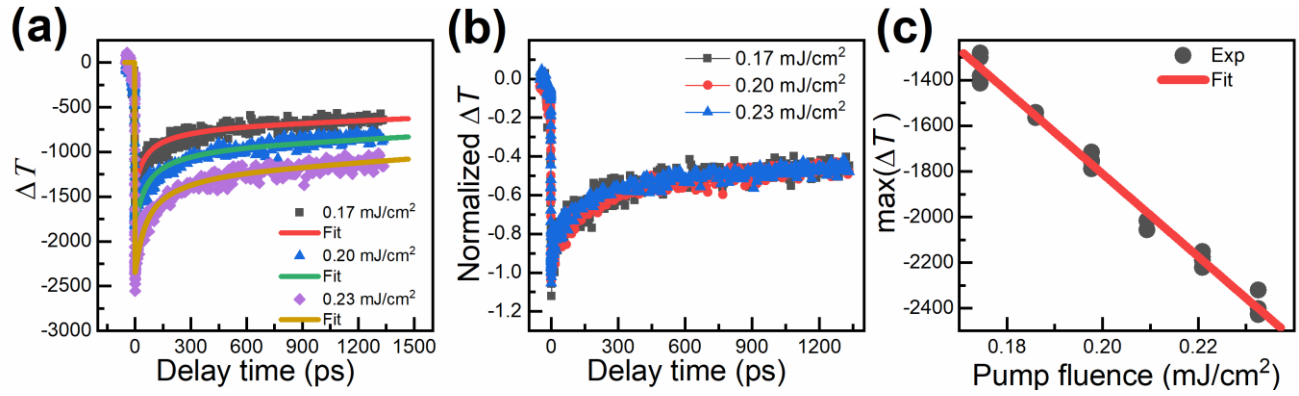

Figure S10. (a) Time-resolved ΔT curve as a function of pump fluence from 400nm-pump 800nm-probe measurements. (b) Normalized transient ΔT curves for different pump fluences. (c) Peak ΔT signal around 0 delay versus pump fluence.

As shown in Figure S11, the time-resolved ΔT curve is independent on the pump polarization, confirming the in-plane isotropy of optical absorption of CIPS crystal.

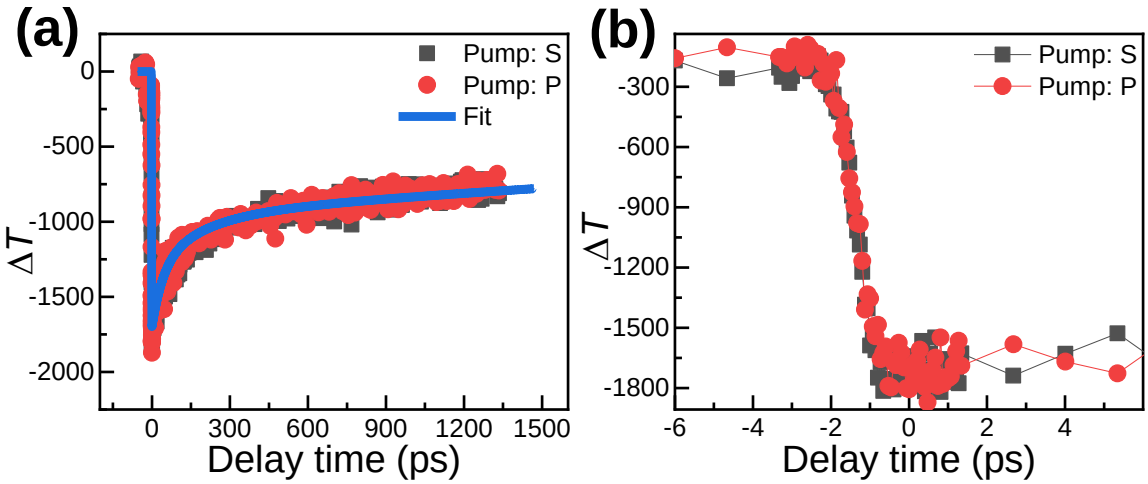

Figure S11. (a) Time-resolved ΔT curve as a function of pump polarization from 400nm-pump 800nm-probe measurements, the probe beam is s-polarized. (b) Zoom-in view of the ΔT curves around 0 delay in (a).

References

1. P. Yu, F. Wang, J. Meng, T. A. Shifa, M. G. Sendeku, J. Fang, S. Li, Z. Cheng, X. Lou and J. He, *CrystEngComm*, 2021, **23**, 591-598.
2. B. Lin, A. Chaturvedi, J. Di, L. You, C. Lai, R. Duan, J. Zhou, B. Xu, Z. Chen, P. Song, J. Peng, B. Ma, H. Liu, P. Meng, G. Yang, H. Zhang, Z. Liu and F. Liu, *Nano Energy*, 2020, **76**, 104972.
3. Y. Hou, M. Qiu, T. Zhang, X. Zhuang, C.-S. Kim, C. Yuan and X. Feng, *Adv Mater*, 2017, **29**, 1701589.